The Impact of Source and Channel Coding in the Communication Efficiency of Wireless Body Area Networks

Richard Mc Sweeney, Christian Spagnol, and Emanuel Popovici
Department of Microelectronics Engineering
University College Cork
Cork, Ireland
richardmcs@ue.ucc.ie, c.spagnol@ue.ucc.ie, e.popovici@ucc.ie

Luigi Giancardi
Department of Biophysical and Electronic Engineering
University of Genoa
Genoa, Italy
luigi.giancardi@ingegneria.studenti.unige.it

***Abstract*—This paper examines the system level energy performance of Wireless Sensor Motes for Electroencephalography (EEG) patient monitoring application by the use of concatenated source and channel coding. The addition of coding in a power constraint system has its advantages by reducing the energy per bit, but it also has its drawback in the cost of the power consumption in the encoding and decoding processes. In this work Huffman code is implemented as the source coding, and a shortened Reed-Solomon code is used for channel coding. The reliability and energy savings of the scheme is presented and the impact of the coding procedure on the communications performance is analyzed. The results show that it is possible to have Bit Error Rate (BER) and compression gains in the system, and that the computational time of purely software oriented implementations are not optimal. Also, the possibility for future extensions of this coding scheme, which would introduce better efficiency and accuracy, are shown. The error patterns that occur in the channel are investigated, and a design space for a possible Hybrid Automatic Repeat reQuest (HARQ) scheme that would minimize the power consumption of this implementation is proposed.**

***Keywords*-Medical application; power reduction; WBAN; Huffman source coding; Reed-Solomon channel coding**

I. INTRODUCTION

The growing interests and developments in the area of wireless sensor networks have opened up many avenues for the applications of such systems in remote monitoring, whether they may be in medical, environment, security, surveillance, or industrial. Patient monitoring and personal healthcare are the focus of this paper, and power optimization in the wireless communication by the use of source and channel coding are presented [1].

Wireless Body Area Network (WBAN) is one type of network that is considered for patient monitoring, where the sensors are distributed around the body and their communications range is limited to the immediate vicinity. They monitor the body and process the acquired data on the battery operated sensor node and then wirelessly transmit them to a monitoring station for further analysis or alarm. The main constraints of such systems include reliability, area, timing, and efficiency, however the main bottleneck that has been generally accepted is the issue of power consumption [2].

The power consumption of the wireless sensor node is distributed among several different areas of the device, where the most common configurations include one or several sensors, a microprocessor/microcontroller/DSP referred as software component, a Custom Digital Signal Processing unit referred as digital hardware component (FPGA/ASIC), memory, and a transceiver. Since one of the most power-consuming devices is the RF module, in order to achieve minimum system power consumption the most effective solution is to buffer the data and operate the transmitter at the highest possible data rate at low duty cycle, thus minimizing the time in which the communication occurs. This can lead to design constraints such as data rate and packet size, and can have a significant effect on the communication efficiency.

Since WBAN in patient monitoring is employed in an indoor environment with communication occurring through the patients body, it is expected that the channel quality would vary significantly. This would require frequent retransmissions, which is not energy efficient if a number of these errors in the corrupted packets can be corrected, thereby mitigating repeat transmissions. This is done by the use of Forward Error Correction (FEC), which introduces systematic redundancies allowing transmission of data at a reduced energy per bit, achieving the same bit error rate. The cost of FEC is additional decoder power consumption at the receiver. To further increase the throughput of the communication, source coding is used to remove redundancies that are inherent in the data. Compression reduces the amount of energy required per bit-of-information in transmission through the channel. Both methods work on the assumption that power savings in the wireless data transmission can be achieved at the expense of power consumption in the encoding/decoding stages of either the processor or the dedicated hardware.

The work proposed in this paper focuses on a software implementation of a source and channel coding scheme on an 8-bit micro-controller. Huffman code is used for com-

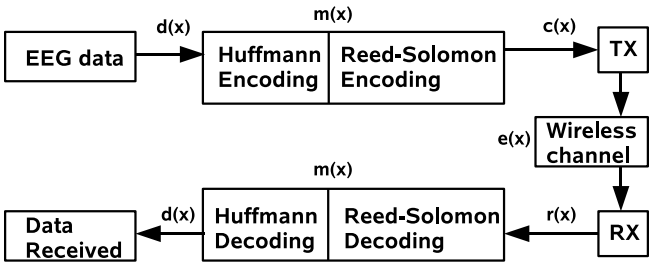

Figure 1. The proposed system flow, illustrating the steps taken from source to sink

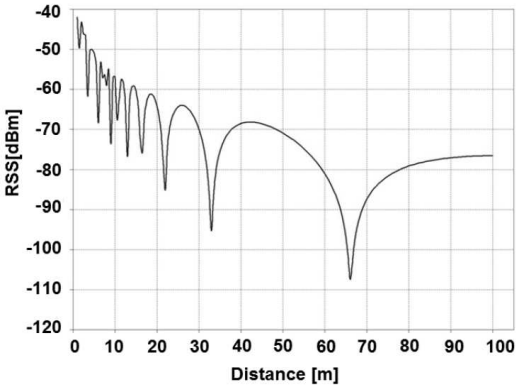

Figure 2. Path loss model for free space with ground reflection at a power level of 0dBm. [5]

pression, and a shortened Reed-Solomon RS(28,24) code over Galois Field GF(2^8) is used for FEC. The system is designed with the applications in the Electroencephalography (EEG) patient monitoring in WBAN architecture. The system itself is implemented on the Tyndall 25mm mote [3] that has an Atmel mega128L processor, and a Nordic nrf2401 transceiver that operate on the 2.4 GHz Industrial, Scientific and Medical (ISM) band. By using the sample EEG data [4], the power measurements are performed in a laboratory environment. The system logical architecture is illustrated in Fig. 1.

Section II discusses the constraints of WBAN and the type of channel that is encountered. Section III of this paper presents the theory and background of source coding and illustrates the factors that affect the quantization and Huffman compression scheme. The theory and methods used in Reed-Solomon channel coding is presented in Section IV. Section V of the paper gives the results of the power reduction and gains in terms of compression and error correcting code. Section VI presents the power savings of using RS to mitigate retransmissions. The conclusion of the findings and the future works are presented in Section VII.

II. WBAN CONSTRAINTS

It is well known that wireless communication has variable channel characteristics that are determined by many factors such as transmitter/receiver power, communication frequency, modulation scheme, reflection, scattering, obstacles, and interferences from other radiating sources. Indoor wireless sensor networks are more susceptible to these factors since the motes operate at lower communication power levels and in environments that contains more obstacles and reflecting sources. The result is that the Receiver Signal Strength (RSS) profile shows pockets of low sensitivity determined by the wave reflections and scattering effects or other factors such as interference and direct obstructions. This in turn affects the Bit Error Rate (BER), and can result in poor communication even at small distances.

Fig. 2 is a path loss model from [5] that illustrates the impact of RSS considering only free space with ground reflections at a power level of 0dBm. It is observed that there is quite a large degradation in the RSS even at small distances.

When implementing wireless communication in WBAN, which has communication distances that are even smaller and that often place the persons body in between the sensor nodes, the problem of reliability in the communication becomes even more pronounced. Therefore it becomes inevitable that severely varying BER would be encountered and the solution becomes that either the transmitter power needs to be increased or some form of error correction needs to be used to alleviate this increase in signal power.

The structure of a WBAN system with a gateway is shown in Fig. 3. The links between the sensors (S) and the master nodes (MN) are the WBAN, and the link with the MN to the monitoring station (MS) is the WLAN. These two types of links have channel characteristic that are different and demand physical (PHY) and media access control (MAC) layers that differ from one another. In the case of WLAN for example, the network can adopt either singlehop or multi-hop schemes, and can have RSS profile that are affected significantly by reflections and scattering from various sources. They may also have different data rate and may use a different frequency for communications than that of WBAN. The WBAN on the other has very small communications range, is usually single-hop architecture and pose a different challenge to the WLAN by often placing direct obstruction (the body) in the line of sight.

One of the works in channel performance and the effect of path loss in the body is presented in [6], where an investigation of the path loss in flat biological tissue at 2.4GHz ISM band is performed. The research draws conclusions on that among the tissue types investigated, the thickness of skin and fat layers have the most variable influence on the path loss, and that proper sizing of the antenna is an important factor. The Research reported in [7] investigates the path loss for the human arm and torso, and path loss parameters were derived from experimental measurements

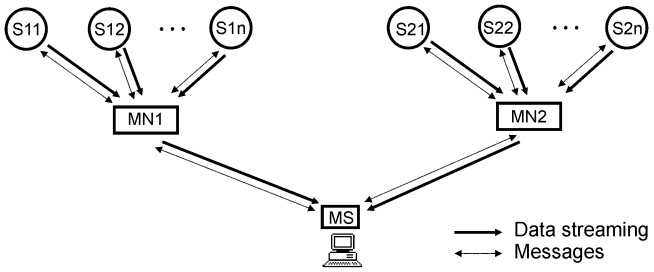

Figure 3. Possible WBAN system connected to WLAN gateway [8]

and are then compared with the model stated in [6]. The study shows that the path loss along the arm and the torso follow the same course but the magnitude of the loss along the torso is higher due to increased absorption, and suggests that the path loss model for a flat homogeneous tissues may underestimate the effect near a human body. These studies show that there is quite a significant amount of degradation in communications efficiency near the human body, and that the designs of WBAN needs to have a high communications power or an appropriate FEC to keep the desired BER.

III. Source Coding

Data compression algorithms can be divided into two families, namely lossless compression and lossy compression techniques [9]. The lossless compression scheme allows perfect reconstruction of the original data, while lossy compression returns an approximation that can achieve better compression rates. The choice of compression scheme used depends heavily on the application and the performance required by the system.

Due to lack of approved standards, medical data is often required by clinical practice physicians to be lossless, and is believed to be an essential requirement for a correct diagnosis. However as it is noted in [10], the diagnosis of 8-bit resolution EEG data gives enough precision to ensure a correct interpretation of the signal by a physician. In this work the EEG data used was sampled with a 12-bit resolution ADC, and an 8-bit micro-controller is used to perform the compression. Basing our system upon the observations made in [10], the ADC data is uniformly quantized from 12-bits to 8-bits. The operation affects the quality of the signal, but also has its advantages by providing easier computations for the 8-bit microcontroller, and by providing less memory requirements for the Huffman codeword LUT.

Huffman code has been chosen due to its simplicity. Given a known probability function, the huffman tree can be built and stored in the SRAM or the flash in the micro-controller. The encoding is performed on the sensor node immediately after data acquisition, using just memory accesses to the codeword LUT. However decoding has higher complexity since it has to assess individual bits to find the corresponding codeword in the LUT. But this is performed on the master node, which is a more powerful machine, hence is not considered critical.

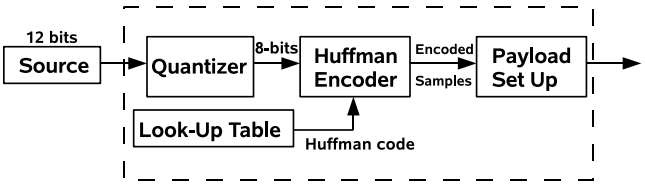

Figure 4. The procedure for source encoding

Therefore for this work a trade-off solution is proposed, where some error (loss) is introduced before the lossless compression stage. The steps of this technique are illustrated in Fig. 4.

The initial step quantizes the 12-bit EEG data to 8-bits, which results in resolution-loss of the amplitudes that is uniformly distributed over the whole dynamic range of the data set. The quantized EEG data is then compressed using the static Huffman encoder, and is subsequently passed into a payload setup, where bit packing is performed. The packet is then either encoded by the channel-encoding scheme, or wirelessly transmitted directly.

A. Quantization

The procedure for the quantization is as follows. The EEG data set is uniformly quantized over the entire dynamic range. The error introduced by the quantizer varies with the maximum amplitude that has to be represented after the quantization, where the peak of the Gaussian distribution plays an integral role in the choice of the quantization interval. This peak amplitude parameter VM is chosen so as to minimize the negative effect of the quantization without significantly affecting the compression performance. The cost-function in (1) is used to select VM.

$$min(VM)\left[J = \alpha Err(VM) + \frac{(1-\alpha)}{Gain(VM)}\right], \quad (1)$$

where the term $Gain(VM)$ is an expression of the source coding gain (explained in details in Section V.A), and the term $Err(VM)$ is an error-function defined by:

$$Err(VM) = \sqrt{\frac{1}{S}\sum_{i=1}^{S}|q_i - d_i|^2 w_i}, \quad (2)$$

where S is the number of EEG samples in the entire training set, $|q_i - d_i|$ is the difference between the quantized value and the original sample, and w_i is the weight-coefficient. i.e. the frequency of occurrence of each value in the database. The α value is a term used to vary the weight between the error and the coding gain.

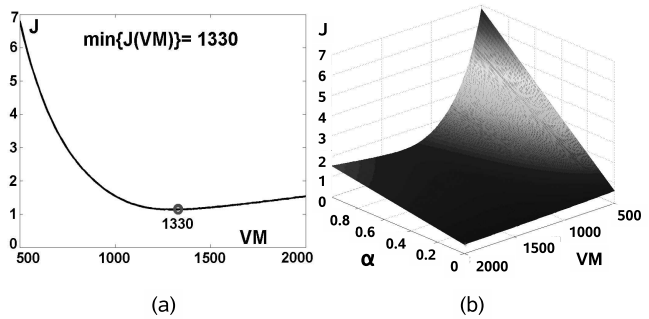

Figure 5. (a) Illustration of the local minima for the 2D Cost function without α (b) 3D Cost function

The plot of the cost function $J(VM, \alpha)$ is shown in Fig. 5(b). It is seen from the figure that this is not a convex function, there are no local minima, and the global minima occurs at α = 0. The conclusion is that α does not contribute to the cost function and is trivial when trying to determine the optimum value of VM. Therefore the cost function is analysed without α. This is illustrated in Fig. 5(a). The minima of this new function $J(VM)$ is found to be at VM = 1330, which is an integer representation of the voltage value that was measured on the sensor.

After the quantization, the data will assume only 256 different values. This is the base-requirement for the next step of the source coding algorithm.

B. Huffmann Coding

Given a discrete source of symbols, the Huffman coding procedure builds for that source a variable-length minimum-redundancy prefix code. The minimum redundancy code is often referred as optimum in the sense that it leads to the lowest possible average codeword length, given N symbols and M digits. It is important to note that for every source there are several optimum codes. We considered only prefix codes, in which a codeword cannot be a prefix of some other codeword, because there is no loss of generality in considering only the prefix ones. In fact it can be shown that given a general optimum code, there exists a prefix code that achieves the same results [10].

The Huffman code tree [11] has a number of leaves proportional to the number of different symbols coming from the discrete source: in this case they are 256, as the Discrete Source is the Quantizer from the previous step. Each leaf contains a string of bits, here called codeword that corresponds to an input symbol. Going from the root deep through the code tree, the symbols become step-by-step less likely, while the related codewords much longer. The average length of the code is defined as,

$$L_{av} = \sum_{i=0}^{N-1} b_i v_i, \qquad (3)$$

where b_i is the codeword, and v_i is the corresponding error probability. The Huffman compression scheme is designed so that the average length of the code is smaller than the uncoded version.

An issue related to this code is that it is impossible to put a limit on the maximum length of a codeword. This is due to fact that the maximum depth of the Huffman tree results from the code-design procedure without any possibility of control. This is a problem since a fixed maximum codeword length is required when working with an 8-bit microprocessor that cannot efficiently handle variables exceeding the size of 8-bits.

To solve this problem a hybrid technique based on the Collapsed Huffman Tree (CHT) is used [10]. Each Huffman codeword larger than length 8-bits are appended a CHT codeword that flag such a case. The resulting final codeword has 16-bits. It has been observed that this does not have a significant negative impact on the average length of the code, because the CHT leaf collects the most unlikely symbols of a given source.

C. Multiple Huffman codes

A possible variant of both classic Huffman and CHT coding is the use of Multiple Huffman codes, i.e. a family of codes that allow the encoder and the decoder to switch between them, by following a certain rule.

By definition, Huffman codes are built (and optimized) to best represent the source of symbols they have been constructed from. This means that such a code has good performances when the training sequence used to build the code is truly representative of the source of symbols that are to be encoded. These considerations imply that a Huffman code is optimum when the source that has been compressed emits the symbols with a homogeneous time-independent distribution. Even if this is true over a large time scale (which is the assumption that the Huffman coding takes), it could be not true over a small time window. In the case of EEG signal processing, it is observed that the distribution of amplitudes differs from normal activity to seizure activity as shown in Fig. 6.

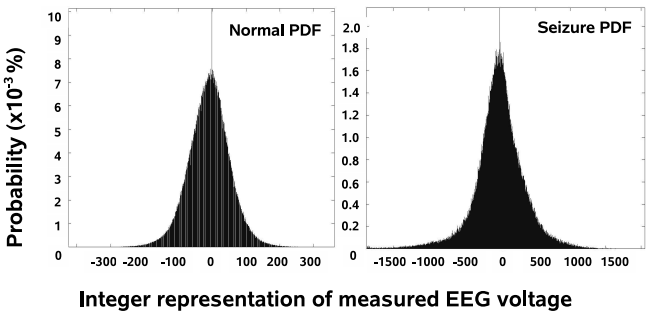

Figure 6. Distribution of amplitudes for a large number of samples taken from normal activity (left) and abnormal activity (right)

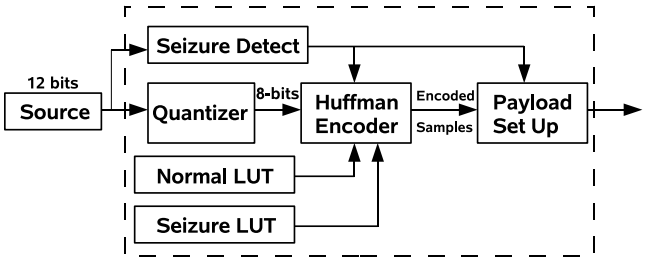

Figure 7. Modified compression scheme for seizure-aware coding

The knowledge of when abnormal activity occurs during a long-term EEG examination would permit to introduce further optimizations to this scheme by the use of multiple Huffman codes. A possible scheme to realize this idea is shown in Fig. 7.

In such a case where the sensor node is aware of the current brain state by means of either an internal procedure or an external indication, the seizure detection block chooses the appropriate Huffman tree to perform the encoding. In this implementation, two Huffman trees are used; one optimized for normal activity, and another one for seizures activity. The codewords are packed in the payload setup as before.

IV. Reed Solomon Channel Coding

The channel code that was chosen for this particular implementation of FEC is the shortened Reed- Solomon (28,24,4) over the Galois Field size of GF(2^8). The RS code [12] is traditionally popular and has been a longtime industry-standard that has found uses in various applications such as satellite communications, Digital Video Broadcasting (DVB), Compact Disks (CD), Digital Versatile Disks (DVD), mass storage, and in wireless communications. The main reasons for such wide-ranging popularity stems from the fact that the RS code has efficient encoding and decoding algorithms, and targets (multiple) burst errors.

A. Reasons for code choice

The RS(28,24,4) over the GF(2^8) is implemented in this scheme due to a variety of reasons. One of the requirements for a power-constrained wireless sensor mote is to operate the most power consuming devices as seldom as possible. The transceiver is then needed to work at as small time frame as possible and at high data rate. These constraints lead to the need of the packet to be small but also at the same time to keep the power consumption of the FEC as low as possible. Therefore the FEC should keep the size small and be computationally easy. This is especially the case for the power-constrained sensor nodes, but is also true for the master node in terms of time taken to decode, which becomes critical in networks that utilize Time-Division Multiple Access (TDMA) protocols.

Various research groups have performed works in the field of feasibility of FEC in Wireless Sensor Networks (WSN). The research done in [13] explores the power estimation of Hamming codes, Convolutional codes (CC), and RS codes and has proposed a framework for the design space of FEC for WSN. It was established that RS codes perform the best in terms of total energy consumed by the motes, and it was seen that packet size of 31 bytes consumes the least amount of power at varying node distances. Through the BER analysis it is shown that the computational power of RS(31,29,3) is the lowest at BER of 10^{-4} and RS(31,27,5) is the lowest at path loss exponent of 4, which equates to a dense noisy environment. The authors of [14] have performed works on power estimation of various BCH, RS, and CC cores on tsmc180nm ASIC process and Xilinx Spartan III FPGA platform. It is shown that the power consumption of linear block codes are much less than that of CC, and that BCH and RS codes are useful in WSN applications. In [15], empirical research has been performed on the BER of the motes in short range ($<$ 1.5 m) WSN, and investigated the packet loss and packet reception of the sensors. The packets are sized to 64 bytes, and through their analysis the authors found that the average number of bit errors in a packet that passed synchronization is 16.68 bits.

The maximum packet size of the burst mode in the nrf2041 is 32 bytes, of which 4 bytes are set for synchronization and address. The maximum size of the packet payload is 28 bytes, and thus the code is built with n=28. The reason for choosing the field size of GF(2^8) is due to the 8-bit micro-controller, where all operations are performed in 8-bit blocks, therefore for ease of operation, and to reduce computational power, the code is built over this field size.

The combination of these reasons not only shows that the choice of RS(28,24) is acceptable for short range WSN, but also justify them from an implementation point of view and that the performance should be similar to the stated figures.

B. Code Architecture

Following the encoding of the EEG data by the Huffman compression scheme on the sensor node, the resulting message $m(x)$ is systematically encoded by the concatenated code and is sent wirelessly through a highly noisy indoor environment. The systematic encoding ensures that the data symbols appear in the codeword, and is expressed, using polynomial notation as follows,

$$c(x) = p(x) + x^{n-k}m(x), \tag{4}$$

where the parity symbols $p(x)$ is chosen such that the codeword $c(x)$ is divisible by the generator polynomial.

Due to the complexity of the Galois field multiplication, and the limitations of the processor to perform only one operation per clock cycle, a bit serial multiplier is used for multiplications in GF(2^8), and a look-up-table is made for inversion to facilitate maximum speed of the operation [16].

Once the packet is received on the master node, the word may be corrupted and this is expressed as $r(x) =$

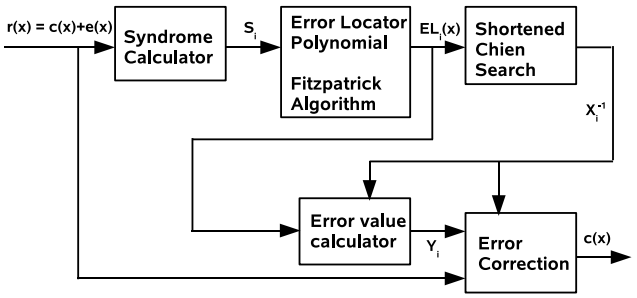

Figure 8. Reed-Solomon Decoder architecture

$c(x) + e(x)$, where $r(x)$ is the received data, $c(x)$ is the codeword, and $e(x)$ is the added channel noise. The RS decoder attempts to correct the errors by means of polynomial operations. The decoding flow can be seen in Fig. 8.

The $(n - k = 2t)$ syndromes S_i are computed and these are used to calculate the Error Locator Polynomial $EL_i(x)$ in an iterative fashion. The commonly used Berlekamp-Massey algorithm [17] for the calculation of the error locator polynomial is here replaced with the Fitzpatrick algorithm [18] due to its faster performance.

Once the Fitzpatrick algorithm has calculated the error locator polynomial, the roots of the polynomial, X_i^{-1} are then found by the shortened Chien search algorithm, which only cycle through the last 28 elements of the GF(2^8) since the code has been shortened to RS (28,24). This observation leads to a considerably shortened computational time for the search calculation.

The resulting roots X_i^{-1} are the inverses of the error locations in the received word and are used for the calculation of the error values Y_i. These error values are calculated without the use of the error evaluator polynomial, as was proposed in [19]. The equation used for the error value calculations is shown in (5).

$$Y_i = \frac{X_i^{-2_t+1}}{EL_{i'}(X_i^{-1})EL_i'(X_i^{-1})}, \quad (5)$$

where $EL_{i'}(x)$ is the update polynomial obtained through the Fitzpatrick algorithm, and $EL_i'(x)$ is the formal derivative of $EL_i(x)$. This algorithm has the advantage over the traditional Forney algorithm [20] in that it does not have to calculate the error evaluator polynomial, thereby saving significant computational effort.

Finally the error is corrected with the use of the error values Y_i and their corresponding error positions X_i^{-1}.

V. Power Measurements and Results

Several implementations are considered for the analysis of the power consumption and the performances of the source and channel codes. These are summarized in Table I.

Table I
Communication Versions Used

Version	Description
Orig.	12-bit EEG data that is transmitted as a 16-bit word
Quant.	Quantized 8-bit EEG data
QH	Quantized 8-bit EEG data with Huffman coding
QRS	Quantized 8-bit EEG data with RS coding
QHRS	Quantized 8-bit EEG data with Huffman and RS coding

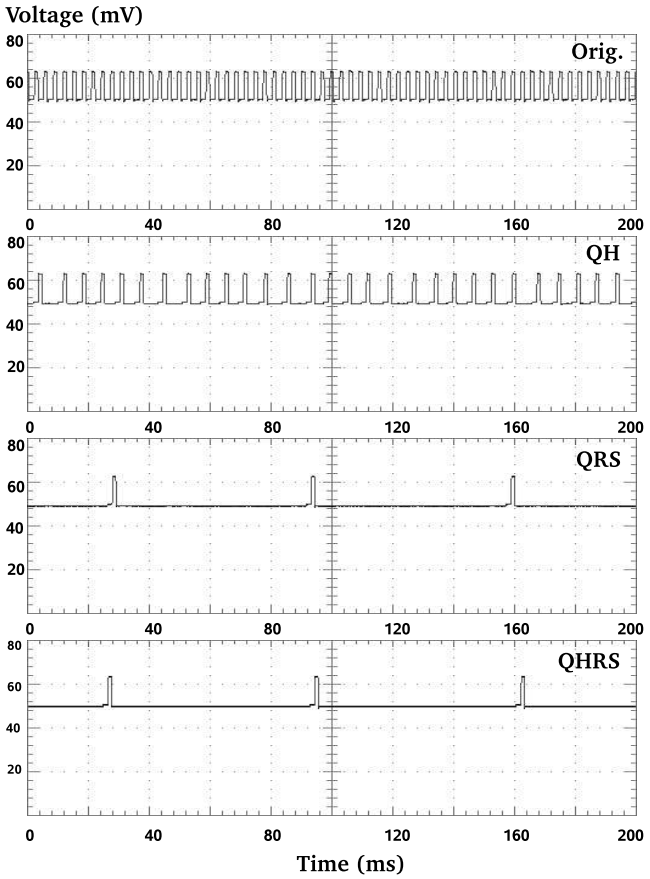

Figure 9. TX system current consumption vs. time

The data is sent wirelessly in burst mode of the nrf2041 at data rate of 250 kb/s and at TX power level of -20dBm. The transmission packets are sized to 32 bytes per packet, with 28 bytes of information payload.

The result current consumption waveforms at the transmitter for the versions 1 to 4 are shown in Fig. 9, where each peak corresponds to a packet being sent. The waveforms are captured via voltage measurement across a 1.7 Ω external resistor with the supply voltage for the Tyndall mote set at 5V. The micro-controller operates on 3.3V, and the transceiver operates on 2.5V. The power consumption of the voltage regulators and the surrounding circuitry are assumed to be negligible. It should also be noted that

Table II
TX POWER AND ENERGY CONSUMPTION

Version	Pac rate (s^{-1})	Pwr TX (mW)	En /Pac TX (mJ)	Pwr RX (mW)	En /Pac RX (mJ)
Orig.	320.5	65.334	0.2038	88.2	0.2752
QH	159.2	59.168	0.3716	88.2	0.5540
QRS	15.21	54.274	3.5683	88.2	5.7988
QHRS	14.79	54.247	3.6678	88.2	5.9635

the development board on which the measurements are performed adds 20.38mV shown in Fig. 9, and needs to be subtracted in order to calculate the power consumption of the mote itself.

Table II summarizes the communication performance and the energy usage of the various schemes at the transceiver power level of -20dBm.

Moving down the column for the different versions, it is observed that the power consumption of the system drops due to a decrease in the packet rate, but the overall energy consumption rises due to the heavier processing demands of the codes. This is due to the limitations of the 8-bit microprocessor to carry out tasks such as efficient bit-wise Galois-Field multiplication, hence high amounts of computational time were introduced that led to reduced packet rate.

In regards to *Orig.* and *QH*, it is observed that *Orig.* has twice the packet rate of *QH* due to the necessary computational effort required by the Huffman coding operation in *QH*. However as seen in Table V, the compression gain works out to be around 60% for most of the time, and therefore the overall throughput of the Huffman encoded data is superior.

In terms of channel coding, it is seen from Table II that communication has higher throughput and hence better performance when the code is not used. However these results do not take into account of the coding gain provided by the FEC nor the channel characteristics. Investigation and results on these aspects are provided in Section V.C and Section VI respectively. It is shown that there are advantages to be had in using FEC in terms of coding gain and in mitigating retransmissions as well as the system power.

A. Compression Performance

The Compression rate is strictly dependent on the average length of the source code, L_{av} as defined in (3). We consider the case of a Huffman tree built using the entire EEG database as the training set with VM=1330 and 8-bit quantization. The compression performance of huffman and collapsed huffman trees are shown in Table III.

It is seen from the table that the efficiency of the CHT technique η_{cht} is lower than the original one η , and the average length of the CHT $L_{av_{cht}}$ is higher than the original L_{av}. Although this is a slight trade-off in the performance

Table III
COMPRESSION FIGURES

Term	Term Description
H = 5.345	Entropy of the signal from quantizer
L_{av}=5.366	Avg. length for the standard Huffman tree
$L_{av_{cht}}$ =5.96	Avg. length for the Huffman tree with the CHT leaf
CHT = 38	Position of the CHT leaf in Huffman tree
η = 0.996	Efficiency of Huffman coding
η_{cht} = 0.897	Efficiency of Huffman coding with the CHT leaf
Mem=507	Memory usage of original LUT in Bytes
Mem_{cht}=38	Memory usage of CHT LUT in Bytes

of the code, it is also seen from the comparison of Mem and Mem_{cht} that there are large memory savings of approximately 92.5% to be had from using CHT.

Although the figures of Table III give the performace of the code that is optimized for the given statistics, it should be noted that the EEG sample used to build the tree contains 20% seizure activity. Since it is rare to see 20% seizure activity in the real case, a test that was devised to explore the compression scheme on various EEG data types. i.e. Seizure and Non-seizure activity. The test consists of transmitting the EEG data in 200 packets through the wireless link, and counting how many information bits are communicated. The average packet length is sized to 24 bytes, where for *QH* one byte is reserved for information on the number of significant bits in the data payload. Fragment 1 holds EEG data activity of seizure prone patients, Fragment 2 holds the data of the patients when in seizure, and Fragment 3 is the normal EEG data of healthy adult subjects. The results are summarized in Table IV.

Table IV
COMMUNICATION PERFORMANCE WITH VARIOUS TYPES OF DATA

FRAGMENT 1	Orig.	Quant.	QH
Total number of packets	200	200	200
Total EEG samples sent	2400	4800	7725
Avg. data payload length (bits)	192/192	192/192	179/184
FRAGMENT 2	Orig.	Quant.	QH
Total number of packets	200	200	200
Total EEG samples sent	2400	4800	3605
Avg. data payload length (bits)	192/192	192/192	177/184
FRAGMENT 3	Orig.	Quant.	QH
Total number of packets	200	200	200
Total EEG samples sent	2400	4800	8690
Avg. data payload length (bits)	192/192	192/192	181/184

The table shows that the quantized values, *Quant.* sends twice as many samples than that of original values *Orig.* and that *QH* achieves even better performance for Fragments 1 and 3. The average data payload length varies for *QH* due to the variable length nature of Huffman coding. To

Table V
HUFFMAN PERFORMANCE WITH VARIOUS EEG

	FRAGMENT 1	FRAGMENT 2	FRAGMENT 3
Avg. length	4.682	9.878	4.1988
$Gain_{cht}$	2.560	1.210	2.850
Gain (%)	60.91	17.35	64.91

summarize the compression performance, the experimental average code length and the corresponding compression gain of the Huffman encoded data for each Fragment can be seen in Table V, where only *QH* is considered. The estimation of the overall compression gain is made using a simple relationship in (6), where 12 is the original resolution of the sample.

$$Gain = \frac{12}{L_{av}}, \qquad Gain_{cht} = \frac{12}{L_{av_cht}}, \tag{6}$$

The results show that coding gain is strictly dependent on the nature of the signal, and if considering that segments such as fragments 1 and 3 occur for more than 99% of the time, the little increment from 8 to 9.878 bits per sample (during the seizure activity) does not affect the compression capabilities of the system over a macro-scale.

B. Multiple Huffman codes

Previous considerations on EEG signal compression with CHT Huffman code show that the coding performances in terms of accuracy and coding gain are strictly related to the composition of the signal entering the encoder. This is inherent to the Huffman-code building algorithm, since seizures (and abnormal activity in general) are less likely than normal activity over a large time scale, than a general activity Huffman code. Even if the encoding scheme here presented can represent any sample with similar level of quality (due to uniform quantization), the performance of the encoder decreases when abnormal activity is present.

In this section, a mixed-activity signal with known occurrences of seizure activity has been encoded using both single and multiple codes. Using the same criterion as (1), the best value for VM (which is a parameter related to quantization intervals size, i.e. to accuracy) are chosen, and two more Huffman codes are built. Based on these, a mixed code is implemented that takes advantage of seizure awareness (available by construction, in this particular case) to introduce further optimization.

The results of the comparison are shown in Table VI, where f is the expected frequency of occurrence of seizures. It is seen that the seizure-aware (multiple Huffman) coding shown in column 4 introduces a double advantage.

First, it encodes the mixed-activity samples with an increased efficiency in comparison to the general code (column 3). This can be observed by looking at the larger number of samples-per-packet sent. Secondly, since the value VM is targeted on the particular class of brain activity, the effects of quantization on signal quality are lower, i.e. the reconstructed (decoded) samples are more similar to the original ones. For example if f = 0.1 (which implies 10% seizure activity), the average error would result to be 6 times lower than the case when the general code is used. This means that the reconstructed signal would have 6 times more accuracy than before. This shows that the multiple-tree scheme brings improvements with respect to the single-tree implementation in terms of compression and the accuracy of the data due to the change in the quantization intervals.

Table VI
A PERFORMANCE COMPARISON BETWEEN DIFFERENT HUFFMAN CODES

Signal	Normal activity	Seizure activity	Mixed activity	
Code	Normal act. code	Seizure act. code	General code	Multiple code
VM	250	1680	1330	Norm, Seiz
ERR (VM)	0.07	0.46	0.64	(1-f)*0.07 + f*0.46
EEG / Pac	25.06	20.03	20.15	24.29

C. Reed Solomon Coding Gain

The coding gain of the RS(28,24) code is usually calculated by setting the desired bit error rate of the uncoded BPSK and the coded BPSK and then measuring the difference between the Signal-to-Noise Ratio (SNR) required to reach such BER. This is achieved by varying the transmitter power levels. However due to the limitations of the transceiver of the Tyndall mote in setting the TX power levels, the SNR was modified by varying the distance between the TX and RX at a constant transceiver power level of -20dBm. It is also noted that the modulation scheme used by the nrf2041 is Gaussian Frequency Shift Keying (GFSK). The results of the measurement are shown in Fig. 10. It should be noted that the distance is inversely proportional to the SNR, and also that the BER decreases with rising SNR.

It is observed visually that as the BER decreases, the gap between the GFSK(uncoded) and that of RS(28,24) become larger. It is interesting to note that there are certain points when the communication becomes worse even at small distances where one would expect lower BER, such as the case at the distance 0.15m. At other distances such as 0.95m to 1.3m, the effect is more prominent. This is due to path loss and reflections from the ground and walls, which interact with the original signal to produce low receiver signal strength. To measure the coding gain of the RS code, the following model is used [21],

$$P_{TX,U}[W] = \eta_U \frac{E_b}{N_0} N \left(\frac{4\pi}{\lambda}\right)^2 d^n, \tag{7}$$

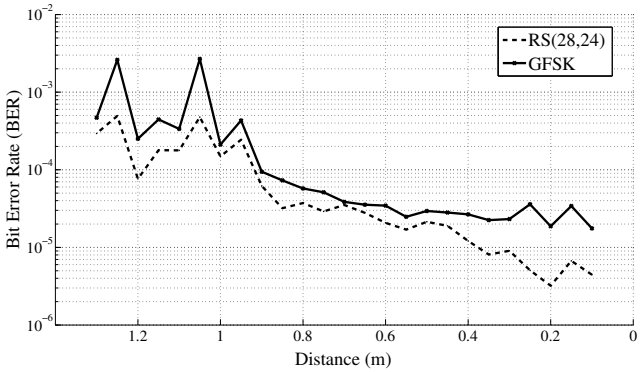

Figure 10. Plot of TX-RX distance vs. Bit Error Rate

where:
η_U = Spectral efficiency (=1 for BPSK)
E_b/N_0 = SNR (energy ratio)
N = Signal noise (Thermal noise*Bandwidth)
λ = Transmitted wavelength
d = Distance between TX and RX
n = Path loss exponent

By placing the coded and uncoded case in proportion, the following relationship is obtained.

$$\frac{P_{TX,RS}[W]}{P_{TX,U}[W]} = \frac{\eta_{MAX}\left(\frac{E_b}{N_0}\right)_{RS} N\left(\frac{4\pi}{\lambda}\right)^2 d^n}{\eta_{MAX}\left(\frac{E_b}{N_0}\right)_{U} N\left(\frac{4\pi}{\lambda}\right)^2 d^n}. \quad (8)$$

Since the same channel and transmitter are used, the above equation can be simplified to,

$$\frac{\left(\frac{E_b}{N_0}\right)_U}{\left(\frac{E_b}{N_0}\right)_{RS}} = \left(\frac{d_{RS}}{d_U}\right)^n. \quad (9)$$

To account for experimental error, the BER values shown in Table VII were chosen to calculate the coding gain. The table illustrates the values of the FEC gain in relation to various environmental conditions expressed as the path loss exponent, where n=2 is for free space, n=3 is for indoor environment, and n=4 is for indoor environment with many obstructions.

It is observed from Table VII that the coding gain rises as the BER is reduced, and that it starts to make larger gains at BER less than 10^{-4}. As mentioned previously, due to the geometrically constrained antenna, the BER is expected to be lower than these values for a system with a better matched antenna and that perhaps these gains actually start at even lower BER. Considering that the frequency of the transceiver used is in a busy communication band (2.4GHz), and the testing is performed in a laboratory setting with plenty of reflections, it is reasonable to assume that the value of the path loss exponent n=3 for this scenario.

Table VII
FEC GAIN FOR VARIOUS ENVIRONMENTAL MODELS

BER	2x10^{-5}	3x10^{-5}	9x10^{-5}	2x10^{-4}	3x10^{-4}
Gain dB (n=2)	5.0263	2.8394	0.5097	0.3855	0.4706
Gain dB (n=3)	7.5394	4.2591	0.7646	0.5782	0.7059
Gain dB (n=4)	10.0526	5.6788	1.0194	0.7709	0.9412

VI. ANALYSIS OF THE CHANNEL

The BER was measured by tallying the number of byte errors that occurred in the communcation at varying distance values of 10cm to 130cm. They are then normalized and presented in terms of overall percentage of errors that occurred in the experiments. These are shown in Fig. 11. To account for the variation in the channel characteristic, the following analysis was performed on four different types of communication based on their bit error rates. They are summarized in Table VIII, where the BER and distance values correspond to the GFSK plot shown in Fig. 10.

Table VIII
CHANNEL SEGMENTS

Segment	Description
10_to_50	Between BER of 2x10^{-5} and 3x10^{-5} (10→50cm)
55_to_90	Between BER of 3x10^{-5} and 1x10^{-4} (60→90cm)
95_to_130	Between BER of 2x10^{-4} and 4x10^{-4} (95→130cm)
105_&_125	BER of 3x10^{-3} (105cm and 125cm)

A. Error Distribution

The plots in Fig. 11 show that a vast majority of the errors that occur are short bursts, where for segments *10_to_50*, *55_to_90*, and *95_to_130*, single byte errors occur at around 60-70% of the time. As the BER rises beyond 10^{-3} (segment *105_&_125*), the error distribution flattens out and is seen that longer burst type errors occur (up to 6 bytes) more frequently. Single byte errors happen less often (40%), and the energy of the noise looks to be spread more around a few bytes. It can also be observed that there is a slight rise in the 28-byte error type in all the segments in this figure. This is considered as packet loss, where an entire packet becomes corrupt and needs to be retransmitted.

From the error distribution, it is also possible to calculate the retransmission rate required for error free communication, and how FEC can be used to reduce this value, hence save energy. Equation (10) is used to calculate the required packet rate.

$$ARQ_m = \frac{\sum_{i=m}^{28}\sum_{j=i}^{28} e_j}{T_{Pac}}, \quad (10)$$

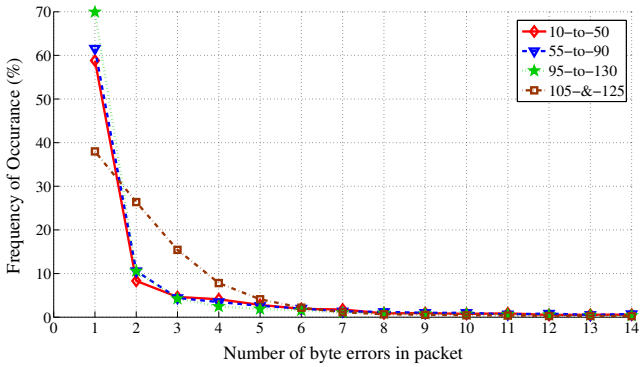

Figure 11. Types of errors occuring for various channel characteristics

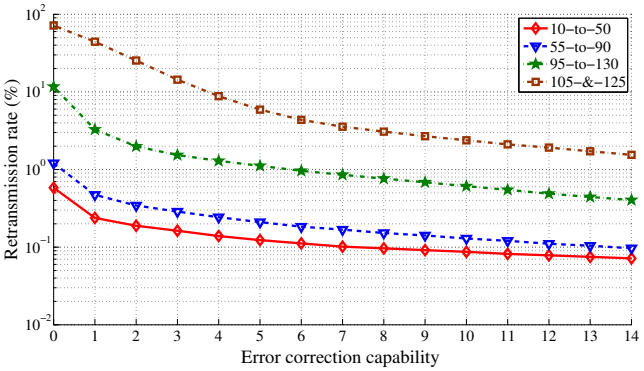

Figure 12. Required retransmission rate for error free communication

where ARQ_m is the retransmission rate, e_j is the error types shown in Fig. 10, T_{Pac} is the total number of packets sent over the channel, and m is the range of error correction capability. The calculation of the retransmission rate is performed and the results are shown in Fig. 12.

The plot shows that with a larger BER such as segment *105_&_125*, the overall retransmission rate is higher of around a factor of 10^2 than that of almost error free communication of segment *10_to_50*. Also it can be observed that the addition of FEC alleviates the need for retransmissions, and this value goes down as the error correcting capability rises.

B. Power savings

Considering that the communication occurs at the same packet rate for the uncoded and the coded versions in the link, it is possible to calculate the power savings of the system. Such assumption can be achieved by using a code thats implemented in hardware such as an FPGA or an ASIC. Therefore one can derive an optimal operating point for FEC that best utilizes the energy when working at varying BER levels at this packet size and data rate. Although the experiment did not directly place any obstructions between the TX and RX, it did however reach a distance in which the receiver sensitivity failed. The experiment was also performed in a closed laboratory environment that provided strong reflections of the transmission. Therefore it is assumed that at higher transmit power (e.g. -10dBm) on a real patient would provide a similar type of scenario, and that the results could be used to design a system specific HARQ.

The power and energy savings are calculated by comparing the original values without any coding with that of increasing error correction capability. Equation (11) is used to calculate the new packet rate Pac_{new_m} from the original packet rate Pac_{orig} and the retransmission requirements RT_m that is in terms of percentage.

$$Pac_{new_m} = \frac{100 Pac_{orig}}{Pac_{orig} + \left(\frac{Pac_{orig} RT_m}{100}\right)}. \quad (11)$$

The total transmission time, T_{tot} is calculated using (12), where T_{TX} is the time taken to transmit a packet.

$$T_{tot_m} = T_{TX} Pac_{new_m}. \quad (12)$$

The average power is found using the information about the power consumption of the micro-controller $P_{\mu C}$, and the power consumption of the transceiver P_{TX}. By knowing the time it takes to transmit the packets in a given window, the product of the respective times and the known powers give the average power consumption of the system by following the relationship shown in (13).

$$\begin{aligned} P_{Avg_m} &= T_{tot_m}(P_{\mu C} + P_{TX}) + (1 - T_{tot_m}) P_{\mu C} \quad (13) \\ &= P_{\mu C} + P_{TX}(T_{tot_m}). \end{aligned}$$

P_{Avg_m} is used to find the average energy E_{Avg_m} that is the average energy consumed by the system to transmit one packet. This is achieved using (14).

$$E_{Avg_m} = \frac{P_{Avg_m}}{Pac_{new_m}}, \quad (14)$$

The energy savings is calculated by taking the difference in the average energy consumption per packet for transmission with no coding, $E_{Avg_{No\_FEC}}$ and that of energy consumption of coded transmission E_{Avg_m}, as shown in (15).

$$E_{Savings_m} = E_{Avg_{No\_FEC}} - E_{Avg_m}, \quad (15)$$

From the energy savings, the average power savings or the difference in terms of power between the uncoded and the coded transmission is calculated at the respective required packet rates as shown in (16).

$$P_{Savings_m} = E_{Savings_m} Pac_{new_m} \quad (16)$$

Fig. 13 illustrates the amount of power saved for the various segment types plotted against the error correcting

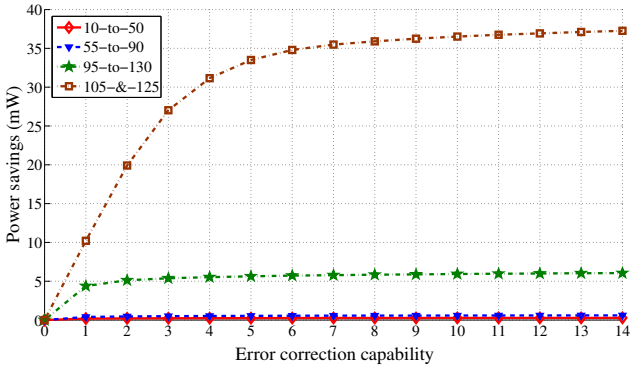

Figure 13. Power savings using shortened Reed-Solomon (28,k,t) with various error correcting capabilities

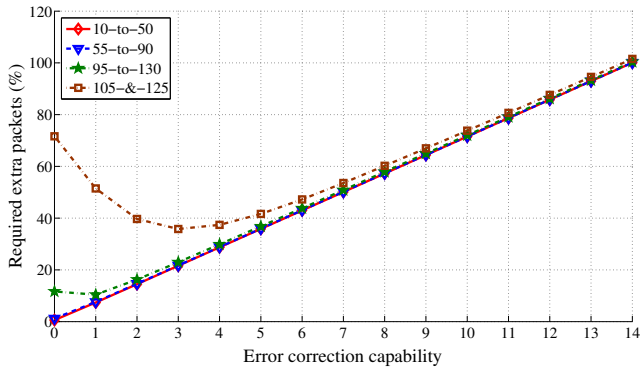

Figure 14. Error correction capability vs. Extra transmissions needed (%)

capability. The zero point on the horizontal axis refers to the case when no FEC is used. It is observed that the power savings approach a certain threshold where the addition of more FEC does not give significant savings. It is also seen that worse the channel, the more benefit in terms of power savings of the wireless sensor mote is achieved by the addition of FEC, and that hardly any power savings are to be had in segments *10_to_50* and *55_to_90*.

Although the addition of FEC can mitigate retransmissions, the cost of this operation is the additional parity bits in the packets, which reduces the overall throughput of the data. Therefore it is also important to consider the cost of total throughput versus the gains achieved by the utilization of FEC. This is illustrated in Fig. 14, where the additional packets needed for a complete transmission of a data set in terms of percentage is shown versus the error correction capability. The point where no error correction is available refers to a link that utilizes just retransmissions.

The figure shows that for segments *10_to_50* and *55_to_90*, the addition of FEC does not result in better throughput. However at a higher BER of segment *95_to_130*, it is observed that there is a slight improvement at m=1. Moving up to segment *105_&_125* shows that there

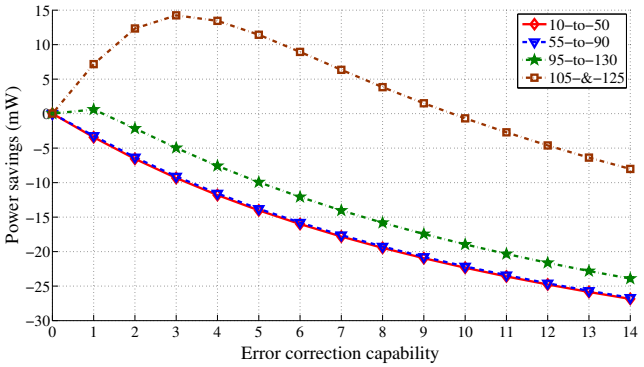

Figure 15. Total TX system power savings using FEC considering throughput

is significant savings as the error correction capability rises, and that the optimum for this BER is at m=3.

The total power savings is calculated by applying (11) to (16), to the results shown in Fig. 13 and Fig. 14. The retransmission requirement RT_m in (11) is modified to incorporate the effect of the throughput. The calculated total power savings are plotted in Fig. 15.

The total power savings shown in the figure strongly reflects the effect that the throughput has on the effectiveness of the FEC. Again it is seen that there are hardly any savings by the FEC at low BER, but it does start to become energy efficient at above BER of 10^{-4}. In segment *95_to_130* it is observed that there is small savings of 0.6mW at m=1, and at segment *105_&_125* the optimum error correction value is at m=3 with savings of 14mW.

VII. Conclusion and Future Work

The possibility of energy savings using a software implementation of a serially concatenated Huffman-RS code was presented. The analysis of the Huffman compression show that EEG compressions gains are achieved in a general case, and that the use of multiple trees for normal and seizure activity present even more gains.

In terms of the mote system performance however, the implementation presented long computational time that made the coding seem less practical. The main reason is due to the limitations of using the 8-bit microprocessor, where the computationally difficult Galois Field operation for the Reed-Solomon code presented significant addition to the processing time. Thus the packet rate was reduced and the energy consumption per packet was increased. This would result in faster depletion of the battery on the real system, which would have a negative effect on the maintenance of the patient monitoring wireless sensor node.

The error distribution for the channel at various BER levels was also performed, and the power savings by the mitigation of retransmissions was calculated. The findings show that FEC can save power at BER levels of 10^{-4} or

higher, and approach optimum values at error correction capabilities of up to 3 bytes for this implementation.

Future work will explore the hardware-software codesign of the Reed-Solomon code along with a HARQ scheme, and also investigate the advantages of joint source-channel coding for medical applications WBAN.

ACKNOWLEDGMENT

The authors wish to thank the Tyndall National Institute for their support in the provision of hardware through the SFI-NAP scheme and for the facilitation of the testing process. This work is funded by SFI-EEDSP for Mobile Digital Health, grant number: 07/SRC/I1169.

REFERENCES

[1] R. Mc Sweeney, L. Giancardi, C. Spagnol, and E. Popovici, "Implementation of source and channel coding for power reduction in medical application wireless sensor network," in *Third International Conference on Sensor Technologies Applications (SENSORCOMM'09)*, Athens, Greece, Jun. 2009, pp. 271–276.

[2] S. Drude, "Requirement and application scenarios for body area networks," in *Mobile and Wireless Communications Summit 2007: 16^th IST*, Budapest, Hungary, Jul. 2007, pp. 1–5.

[3] Tyndall National Institute, Available at: http://www.tyndall.ie/mai/25mm.htm.

[4] R. G. Andrezjak, K. Lehnertz, F. Mormann, C. Rieke, P. David, and C. Elger, "Indications of nonlinear deterministic and finite dimensional structures in time series of brain electrical activity: Dependence on recording region and brain state," *Physical Review E*, vol. 64, no. 6, p. 061907, Nov. 2001.

[5] T. Stoyanova, F. Kerasiotis, A. Prayati, and G. Papadopoulos, "A practical rf propagation model for wireless network sensors," in *Third International Conference on Sensor Technologies Applications (SENSORCOMM'09)*, Athens, Greece, Jun. 2009, pp. 194–199.

[6] L. Roelens, W. Joseph, and L. Martens, "Characterization of the path loss near flat and layered biological tissue for narrowband wireless body area networks," in *International Workshop on Wearable and Implantable Body Sensor Networks, (BSN'06)*, Cambridge, Massachusetts, U.S.A, Apr. 2006, pp. 50–56.

[7] E. Reusens, W. Joseph, G. Vermeeren, and L. Martens, "On-body measurements and characterization of wireless communication channel for arm and torso of human," in *International Workshop on Wearable and Implantable Body Sensor Networks, (BSN'07)*, Aachen University, Germany, Mar. 2007, pp. 264–269.

[8] S. Marinkovic, C. Spagnol, and E. Popovici, "Energy-efficient tdmabased mac protocol for wireless body area networks," in *Third International Conference on Sensor Technologies Applications (SENSORCOMM'09)*, Athens, Greece, Jun. 2009, pp. 604–609.

[9] A. Gersho and R. M. Gray, *Vector Quantization and Signal Compression*. Norwell, MA: Kluwer Academic Publishers, 1992.

[10] G. Antoniol and P. Tonella, "Eeg data compression techniques," *IEEE Transactions on Biomedical Engineering*, vol. 44, 2, pp. 105–114, Feb. 1997.

[11] D. A. Huffman, "A method for the construction of minimum-redundancy codes," *Proceedings of the I.R.E.*, vol. 40, 9, pp. 1098–1101, Sep. 1952.

[12] I. Reed and G. Solomon, "Polynomial codes over certain finite fields," *Journal of the Society for Industrial and Applied Mathematics*, vol. 8, 2, pp. 300–304, Jun. 1960.

[13] S. Chouhan, R. Bose, and M. Balakrishnan, "A framework for energy-consumption-based design space exploration for wireless sensor nodes," *IEEE Transactions on Computer-Aided Design of Integrated Circuits and Systems*, vol. 28, 7, pp. 1017–1024, Jul. 2009.

[14] G. Balakrishnan, M. Yang, Y. Jiang, and Y. Kim, "Performance analysis of error control codes for wireless sensor networks," in *International Conference on Information Technology, (ITNG'07)*, Las Vegas, Nevada, USA, Apr. 2007, pp. 876–879.

[15] A. Willig and R. Mitschke, "results of bit error measurements with sensor nodes and casuistic consequences for design of energy-efficient error control schemes," in *Proc. 3rd European Workshop on Wireless Sensor Networks*, Zrich, Switzerland, Jan. 2006, pp. 310–325.

[16] S. Lin and D. Costello, *Error Control Coding: Fundamentals and Applications*. New Jersey, USA: Prentice Hall, 1983.

[17] J. L. Massey, "Shift register synthesis and bch decoding," *IEEE Transactions on Information Theory*, vol. 15, pp. 122–127, Jan. 1969.

[18] P. Fitzpatrick and S. Jenning, "Comparison of two algorithms for decoding alternant codes," *Applicable Algebra In Engineering, Communication and Computing*, vol. 9, 3, pp. 211–220, 1998.

[19] E. Popovici, "Algorithms and architectures for decoding reed-solomon and hermitian codes," Ph.D. dissertation, University College Cork, University College Cork, Cork, Ireland, 2002.

[20] G. D. Forney, "On decoding bch codes," *IEEE Transactions on Information Theory*, vol. 11, pp. 393–403, Oct. 1965.

[21] S. L. Howard, C. Schlegel, and K. Iniewski, "Error control coding in low-power wireless sensor networks: When is ecc energy-efficient?" *EURASIP Journal on Wireless Communications and Networking*, vol. 2006, 2, pp. 1–14, 2006.